J Neuropathol Exp Neurol. Author manuscript; available in PMC 2016 May 25.

Published in final edited form as:

J Neuropathol Exp Neurol. 2008 July ; 67(7): 687–701. doi:10.1097/NEN.0b013e318181b8ae.

Proepileptic Influence of a Focal Vascular Lesion Affecting Entorhinal Cortex-CA3 Connections After Status Epilepticus

Giuseppe Biagini, MD, **Enrica Baldelli, PhD**, **Daniela Longo, MSc**, **Miranda Baccarani Contri, DSc**, **Uliano Guerrini, PhD**, **Luigi Sironi, PhD**, **Paolo Gelosa, MSc**, **Isabella Zini, DSc**, **David S. Ragsdale, PhD**, and **Massimo Avoli, MD, PhD**

Dipartimento di Scienze Biomediche, Università di Modena e Reggio Emilia, Modena (GB, EB, DL, MBC, IZ); Dipartimento di Scienze Farmacologiche, Università di Milano (UG, LS, PG); IRCCS Monzino Centro Cardiologico (LS), Milan, Italy; Montreal Neurological Institute and Departments of Neurology and Neurosurgery and Physiology, McGill University (DSR, MA), Montreal, Canada; and Dipartimento di Medicina Sperimentale (MA), Università di Roma “La Sapienza,” Rome, Italy

Abstract

In limbic seizures, neuronal excitation is conveyed from the entorhinal cortex directly to CA1 and subicular regions. This phenomenon is associated with a reduced ability of CA3 to respond to entorhinal cortex inputs. Here, we describe a lesion that destroys the perforant path in CA3 after status epilepticus (SE) induced by pilocarpine injection in 8-week-old rats. Using magnetic resonance imaging, immunohistochemical, and ultrastructural analyses, we determined that this lesion develops after 30 minutes of SE and is characterized by microhemorrhages and ischemia. After a longer period of SE, the lesion invariably involves the upper blade of the dentate gyrus. Adult rats treated with subcutaneous diazepam (20 mg kg^{-1} for 3 days) did not develop the dentate gyrus lesion and had less frequent spontaneous recurrent seizures ($p < 0.01$). Young (3-week-old) rats rarely (20%) developed the CA3 lesion, and their spontaneous seizures were delayed ($p < 0.01$). To investigate the role of the damaged CA3 in seizure activity, we reinduced SE in adult and young epileptic rats. Using FosB/ΔFosB markers, we found induction of FosB/ΔFosB immunopositivity in CA3 neurons of young but not in adult rats. These experiments indicate that SE can produce a focal lesion in the perforant path that may affect the roles of the hippocampus in epileptic rats.

Keywords

Hemorrhage; Hippocampus; Immediate early genes; Ischemia; Magnetic resonance imaging; Pilocarpine; Temporal lobe epilepsy

Send correspondence and reprint requests to: Giuseppe Biagini, MD, Dipartimento di Scienze Biomediche–Sezione di Fisiologia, Via Campi 287, Modena 41100, Italy; gbiagini@unimore.it.

Drs. Biagini, Baldelli, and Longo equally contributed to this study.

INTRODUCTION

The role of the hippocampus in temporal lobe epilepsy (TLE) remains unclear (1, 2). Kindling experiments have shown that the hippocampus is rather slow to develop seizures compared with other limbic areas (3). Conversely, studies assessing the expression of immediate early genes have revealed that c-Fos is rapidly expressed in the hippocampus of kainic acid–treated rats (4) and in a model of self-sustaining limbic status epilepticus (SE) (5). Moreover, intense c-Fos staining was found in the hippocampal formation (i.e. entorhinal cortex [EC], dentate gyrus, hippocampus, and subiculum) 30 minutes after spontaneous seizures in pilocarpine-treated mice (6). Thus, the hippocampus is readily recruited during SE and during subsequent recurrent seizures.

We have previously reported that the various hippocampal regions are differentially affected by seizures in pilocarpine-treated animals (7). Both CA1 and CA3 are extensively stained with antibodies against FosB/ΔFosB antigens 24 hours after SE induction, implying that the entire hippocampus participates in epileptic activity. In contrast, after the occurrence of spontaneous recurrent seizures, the CA3 region is devoid of FosB-/ΔFosB-positive neurons. This observation remains unexplained because pyramidal neurons are only partially lost after SE in this model (7). In addition, inputs from the dentate gyrus to CA3 are preserved, as are the responses of dentate granule cells to epileptogenic stimuli (7). Interestingly, in the kindling paradigm, the granule cells develop transient inhibitory properties due to the appearance of a γ-aminobutyric acidergic phenotype, which reduce the probability of CA3 pyramidal cell activation (8). Evidence of similar changes has yet to be obtained in the pilocarpine model.

The downregulation of CA3 activity in the pilocarpine model is intriguing. In vitro studies in normal rats have shown that CA3 is the most responsive hippocampal region in combined hippocampus-EC slices stimulated with 4-aminopyridine or pilocarpine (1). In fact, neuronal synchronous activation is first recorded in CA3 and resembles the interictal spiking observed in TLE patients. This interictal-like activity is followed by ictal-like discharges that are generated in EC and spread to other areas. Notably, ictal-like discharges disappear after a few hours but are reinstated by disconnecting the hippocampus from EC, a process that prevents the spread of interictal-like activity to the EC (1). These results suggest that the hippocampus controls the propensity of EC networks to generate ictal-like discharges and led us to postulate that an impairment of hippocampal outputs might facilitate seizures (1). Consistent with this hypothesis, pilocarpine-treated rats show a reduction in the occurrence of interictal activity and a decreased response of the CA3 region (1,7). These phenomena remain unexplained.

While investigating the role of astrocytes in epileptogenesis, we recently found gliosis in the stratum lacunosum–moleculare of CA3 in rats 3 weeks after pilocarpine treatment (9). These data suggested the possibility that a previously uncharacterized lesion may develop in the perforant path (PP) terminal field of the CA3 region after pilocarpine-induced SE. Here, we tested this hypothesis in rats treated with pilocarpine using several neuronal, glial, and vascular lesion markers. We have discovered an area of focal ischemia-like pannecrosis centered in the CA3 stratum lacunosum–moleculare that is associated with decreased

activation of pyramidal neurons. Interestingly, this lesion is accompanied by an increased propensity of pilocarpine-treated animals to produce spontaneous seizures.

MATERIALS AND METHODS

Animals and Treatments

Young (3-week-old) and adult (8-week-old) male Sprague-Dawley rats (Harlan, S. Pietro al Natisone, Italy) were used. They were housed under controlled temperature (23 ± 1°C), humidity (~60%), and daylight cycle (light from 7 AM to 7 PM). All experimental procedures were approved by the respective institutional animal care committees. A first set of experiments were conducted in adult rats treated with intraperitoneal pilocarpine (380 mg kg^{-1}), as reported by Biagini et al (7, 9). A second set of experiments involved both adult and young rats. In these experiments, young rats were treated with 200 mg kg^{-1} of intraperitoneal pilocarpine (10). To prevent discomfort caused by peripheral muscarinic receptor stimulation, rats were treated with subcutaneous scopolamine methylnitrate (1 mg kg^{-1}) 30 minutes before the pilocarpine injections. Animal behavior was monitored after pilocarpine injection and scored according to Racine classification (11). Rats that did not reach a Stage 5 response to pilocarpine (i.e. continuous tonic-clonic seizures) were not used for the study. A Stage 5 response for 30 minutes was considered to be SE. In adult rats, seizures were discontinued after 180, 120, 60, or 30 minutes with intraperitoneal diazepam (20 mg kg^{-1}) (9). A subgroup (hereafter named “neuroprotected”) that experienced 30-minute SE was treated with subcutaneous diazepam (20 mg kg^{-1}) for 3 additional days. In young rats, the seizures were discontinued by diazepam injection after 60-minute SE to improve survival. Control rats were injected intraperitoneally with saline. Non-epileptic control and pilocarpine-treated epileptic rats were killed 1 to 3 days or 1 to 8 weeks after the initial injection.

In a third set of experiments, SE was reinduced in epileptic rats that had been previously treated with pilocarpine at 3 weeks (young) or 8 weeks (adult) of age. For these studies, we followed the protocol of repeated injections of subthreshold pilocarpine doses proposed by Glien et al (12). In brief, after scopolamine administration, we injected a 200-mg kg^{-1} pilocarpine dose. In the absence of seizure activity, we injected additional 100-mg kg^{-1} doses every 30 minutes (up to a maximum of 6 repeated treatments) until SE was attained. Status epilepticus was then discontinued after 60 minutes as previously reported. Age-matched nonepileptic control rats were used to determine possible changes in the threshold for seizures of epileptic rats. In these experiments, the animals were killed 24 hours after the pilocarpine treatment.

Monitoring of Spontaneous Seizures

After recovering from SE, every animal was video-recorded 8 hours per day, 7 days a week to identify the time of appearance and to estimate the frequency of spontaneous seizures. The seizures consisted of facial automatisms, head nodding, forelimb clonus, rearing, and eventual generalization, but only Stage 5 (i.e. generalized tonic-clonic seizures) were scored.

Nuclear Magnetic Resonance Imaging

For magnetic resonance imaging evaluations, rats were anesthetized with 2% isoflurane in 70% N_2/30% O_2 and investigated using a 4.7-T Bruker spectrometer (AMX3). A 3-orthogonal-plane, gradient-echo scout acted as a geometric reference; then, axial T2-weighted (T2W), reference, and diffusion-weighted images were acquired with eight 1.5-mm-thick contiguous slices and a field of view of 56 × 56 mm^2 that contained the whole brain. The fast spin-echo T2W (Bruker RARE), with 16 echoes per excitation, 10-millisecond interecho time, 85-millisecond equivalent echo time, and 4-second repetition time was acquired with 256 × 256 points providing an in-plane resolution of 220 μm. The spin-echo reference and diffusion-weighted images (echo time, 40 milliseconds; repetition time, 1 second) were acquired with 128 × 128 points, resulting in an in-plane resolution of 440 μm. Diffusion weighting was obtained by adding to a spin-echo multislice sequence two 10-millisecond-long, 24.7-millisecond-spaced, 8-G cm^{-1} rectangular gradients, giving a *b* value of approximately 1,000 seconds mm^{-2}. Four averages were acquired in 8.5-minute per gradient direction. Trace of diffusion tensor maps was computed from reference and diffusion-weighted images.

Histopathology and Immunohistochemistry

For tissue analysis, rats were anesthetized with chloral hydrate (450 mg kg^{-1}, i.p.) and perfused via the ascending aorta with 100 ml of saline, followed by 100 ml of 4% paraformaldehyde and picric acid (0.3%) dissolved in 0.1 mol L^{-1} of phosphate buffer (pH 6.9). Brains were then postfixed overnight in the same fixative at 4°C, and, after cryoprotection by immersion in 15% and 30% sucrose-phosphate-buffered solutions, were frozen and cut horizontally with a freezing microtome in serial 50-μm-thick sections. Sections were incubated with several antibodies (Table). Immunohistochemistry was performed using the avidin-biotin complex technique and diaminobenzidine as chromogen, as previously described (7, 9). Nerve fibers were stained with the Black-Gold method (13). Degenerating neurons were visualized with Fluoro-Jade (Histo-Chem, Inc., Jefferson, AR), as previously described (7). All the chemicals were from Sigma-Aldrich (Milan, Italy) unless otherwise specified.

Image Analysis

Stained sections were analyzed by the KS300 (Carl Zeiss, Vision, Munich, Germany) image analysis software, as previously detailed (7, 9, 14). Briefly, fields (1.18 mm^2) of glial fibrillary acidic protein (GFAP), microtubule-associated protein 2 (MAP2), laminin, and metabotropic glutamate receptor 2/3 (mGluR2/3) immunoreactivity were acquired in CA3 by an Axioskop (Carl Zeiss) microscope using a Sony charge-coupled device-IRIS BW video camera. After having selected the GFAP-, MAP2-, and mGluR2/3-specific immunoreactivities, areas of loss of immunostaining were delimited and measured in 5 serial sections separated from each other by 0.3 mm. Volumes were calculated as $V = \sum 1/3\,[r_i^2 + r_{i+1}^2 + r_i \times r_{i+1})\pi d]$ for n−1 serial levels, in which r_i is the radius at the *i*th level and *d* is the interlevel distance (14). Laminin immunoreactivity was measured as field area values, corresponding to the summing up of areas of the specific profiles obtained after

discrimination from the background staining. Background values were obtained in hippocampal areas devoid of specific immunostaining.

Electron Microscopy

Perfusion-fixed brains from rats exposed to 30-minute SE and control rats were removed 1 or 3 days after treatment and sectioned by a vibratome in 1-mm-thick horizontal slices that were postfixed at 4°C for a further day using 2.5% glutaraldehyde in Tyrode solution (pH 7.2). After isolation of the hippocampus, the samples were washed in Tyrode solution, postfixed with 1% osmium tetroxide for 2 hours at room temperature, dehydrated in graded ethanols, and embedded in Spurr resin (Polysciences, Inc., Warrington, PA). Semithin sections (1-μm thick) were cut on a Reichert-Jung ultramicrotome, postpolymerized on a 150°C hot plate, and finally observed under a Zeiss Axiophot microscope (Zeiss) to identify the hippocampal structures. Thin sections cut from the same cross-oriented samples were collected on 200 mesh nickel grids, stained with uranyl acetate and lead citrate, and examined using a JEOL 1200 EX II electron microscope.

Data Analysis

Statistical analysis was performed using the Statistical Package for the Social Sciences, version 8.0 (SPSS, Chicago, IL). Results were analyzed with 1-way analysis of variance and the Fisher least-significant-difference method for multiple comparisons. The Kaplan-Meier method was used to estimate the time-dependent changes in lesion detection and the onset of Stage 5 spontaneous seizures after SE (11). These curves were compared by the logrank test. Data are presented as mean ± SEM and were considered significant if $p < 0.05$.

RESULTS

Microhemorrhages in CA3 After SE

We screened for the presence of damage in rats exposed to 180-minute SE (Fig. 1) at 7 days after pilocarpine injection (n = 11) and found microhemorrhages in 5 of 11 rats. These lesions consisted of extravasated erythrocytes close to the walls of markedly dilated arteries (Fig. 1B; arrows) or perivascular erythrocyte cuffs (Fig. 1B; arrowheads). In addition, we observed a sector of extensive cell loss localized in the upper blade of the dentate gyrus (Fig. 1B; double arrows). This lesion was found consistently in all pilocarpine-treated rats (n = 11) and contrasted with the apparent integrity of the other sectors of the dentate gyrus (compare the lower blades of control and pilocarpine-treated rats in Figs. 1A and B, respectively). Areas of neuronal loss were also detected in CA3 in 2 of 11 rats (Fig. 1B; asterisk). Interestingly, these areas contained branches (Fig. 1B; double arrowheads) of the dilated blood vessel located in the stratum lacunosum-moleculare (Fig. 1B; arrowheads). Fluoro-Jade staining of sections from rats killed 1 to 3 days after SE (n = 4 and 6, respectively) revealed clusters of necrotic granule cells in the upper blade of the dentate gyrus (Fig. 1C; arrow) corresponding to the sector of cell loss close to the lesion centered in the CA3 stratum lacunosum-moleculare (Fig. 1B; double arrows). This finding contrasted with the sparse distribution of the other necrotic cells in the hilus of dentate gyrus (Fig. 1C; double arrows) or in other sectors of the granule cell layer (Fig. 1C; arrowheads).

In CA3, we also found an increase in immunostaining for heme oxygenase 1, an enzyme that is mainly expressed in microglial cells involved in removing hemoglobin from tissue (15) (compare the control immunostaining in Fig. 2A, n = 4, with that obtained from pilocarpine-treated rats in Fig. 2B, n = 11). Some heme oxygenase 1-positive cells were localized in the wall of the dilated vessels (Fig. 2B; arrow). These data prompted us to look for vascular wall lesions that might explain the presence of microhemorrhages. An antibody against laminin (16) detected increased immunostaining of vessel walls after SE especially in the CA3 subfield (compare the control staining in Fig. 2C with that in a pilocarpine-treated rat; Fig. 2D) but never in the EC (compare the control staining in Fig. 2E with that in the pilocarpine-treated rat in Fig. 2F).

Evidence of Ischemic-Like Lesion in the CA3 Region

Next, we looked for concomitant ischemia in CA3 by evaluating the integrity of glial cells (17, 18) in rats killed 3 (n = 6), 7 (n = 8), or 14 (n = 8) days after 180-minute SE. Using an antibody against GFAP (Fig. 2G), we identified a well-defined area of astrocyte loss (Fig. 2G; arrows) surrounding the microhemorrhage in the CA3 subfield (Fig. 2G; arrowhead) in pilocarpine-treated rats 3 days after SE. This focal loss of GFAP immunostaining was found in all pilocarpine-treated rats 3 or 7 (Fig. 2H; top panel) days after SE, including in animals that did not have red blood cell extravasation. We did not detect any areas of GFAP loss (Fig. 2H; top panel) in rats killed 14 days after SE. In fact, the area of GFAP loss in rats after a week of SE was significantly decreased (−75%; $p < 0.01$) versus rats examined 3 days after SE (Fig. 2H; top panel). Statistical analysis using the logrank test showed significant differences ($p < 0.01$) between rats studied 3 and 7 days after SE and the control group (n = 4). In contrast, rats studied 14 days after SE were significantly different ($p < 0.01$) from the other pilocarpine-treated rats but not from controls. These changes coincided with a significant increase (~500% of basal values; $p < 0.01$) in laminin immunoreactivity that was evident 3 days after SE but not present 2 weeks later (Fig. 2H; middle panel). No changes were observed in the EC (Fig. 2H; bottom panel).

Evaluation of Nerve Fiber Loss in the CA3 Region

We also examined the integrity of axons reaching the stratum lacunosum-moleculare by staining myelin with the Black-Gold method (n = 4, controls; n = 11, pilocarpine-treated). Fibers of the temporodentate or temporoammonic projections of the PP (identified as TD and TA, respectively, in Fig. 3A) were clearly delineated in horizontal sections of control hippocampi. By contrast, in all rats experiencing 180-minute SE, the PP terminal field in the CA3 stratum lacunosum-moleculare was undetectable with Black-Gold staining (Fig. 3B). This unstained area (Fig. 3B; asterisks) was seed-shaped, with the bottom filling the stratum lacunosum-moleculare in CA3 and the top covering the adjacent dentate gyrus edge and the temporoammonic projection, which seemed to be truncated when approaching CA3. In addition, fibers of the temporodentate projection that reach the upper blade tip of the dentate gyrus were also completely damaged. Higher magnification revealed varicosities (arrows in Fig. 3D; the control staining in a corresponding area is shown in Fig. 3C) along the myelin sheath of nerve fibers located at the border of the lesion. These varicosities were also identified in the molecular layer of the dentate gyrus (arrows in Fig. 3F; the corresponding

control region is shown in Fig. 3E), which is reached by temporodentate projections of the EC (19).

Distribution of Lesions in Extrahippocampal Regions

By comparing the pattern of GFAP immunostaining in pilocarpine-treated rats exposed to 180-minute SE with control sections, we also detected lesions similar to those found in the hippocampus in other brain regions (Fig. 4A and B; obtained from rats killed 3 days after SE; n = 6). In particular, loss of GFAP immunostaining was evident in the piriform and insular cortex (Fig. 4B; arrowhead) and in regions of the ventral forebrain such as the basolateral amygdala and endopiriform nucleus (not shown). Other areas of GFAP loss were consistently found in the substantia nigra pars reticulata. Microhemorrhages were always observed in the hypothalamus and thalamus and sometimes in the septum and striatum; however, these microhemorrhages were never associated with loss of GFAP immunostaining (Fig. 4B; arrows).

Limiting SE to 30 minutes attenuated extrahippocampal lesions (Fig. 4C). Specifically, after 30-minute SE, we detected hemorrhagic lesions in the hippocampus in only 2 of 8 rats. Clearly defined areas of GFAP loss were detected in the piriform (4/8 rats), insular (4/8), and perirhinal (1/8) cortices. Conversely, the amygdala, endopiriform nucleus, and substantia nigra were preserved. The hippocampus was consistently affected; focal GFAP loss was detected in 7 of 8 rats studied 3 days after 30-minute SE. The extent of this hippocampal lesion, however, was greatly reduced (not quantified in these experiments). Interestingly, even when the area of GFAP loss was very small, we found a large increase in laminin immunoreactivity (compare Figs. 4F and I, obtained from a pilocarpine-treated rat exposed to 30-minute SE, with Fig. 4D and G from a control rat) in the stratum lacunosum-moleculare of CA3 of all rats (n = 8). This change in laminin immunostaining was restricted to vessels located in CA3 and was independent of the presence or absence of GFAP loss (Fig. 4H, I). In contrast, changes in laminin immunoreactivity observed in other extrahippocampal areas (Fig. 4E, F) were not as striking or localized as they were in CA3.

Ultrastructural Analysis of the Vessel Damage

We analyzed at the ultrastructural level the development of vascular lesions in the CA3 of rats exposed to 30-minute SE and killed 1 (n = 3) or 3 days later (n = 3) compared with control nonepileptic rats (n = 3). As shown in Figure 5, minimal changes suggestive of neuron/astrocyte swelling were detected in the stratum lacunosum-moleculare 24 hours after SE (compare Fig. 5A, obtained from a control rat, and Fig. 5B). In contrast, 3 days after SE, there were marked changes in the morphology of brain capillaries and surrounding tissue consisting of (1) the appearance of several microvilli on the surface of endothelial cells (arrows in Fig. 5C), which suggests activation of transport processes; (2) presence of large vacuoles within the endothelial cell cytoplasm (Fig. 5C, asterisks), which also indicates maximal activation of intracellular transport; (3) detachment of pericytes from the vessel wall (“P” in Fig. 5C), probably migrating within the parenchyma; (4) marked swelling of astrocyte end-foot processes (“AS” in Fig. 5C); (5) axon degeneration (arrowheads in Fig. 5C), indicated by myelin sheath splitting, axon shrinkage, and axoplasm condensation; and (6) tissue edema, indicated by enlargement of the periaxonal space.

Time Course of the CA3 Lesion

To characterize the development of the lesion in the hippocampus, we investigated pilocarpine-treated rats using magnetic resonance imaging (Fig. 6). Brain lesions were detected in T2W images (Fig. 6A) and in apparent diffusion coefficient of water maps (Figs. 6B, C). Changes in T2W images, detected as bright zones of signal hyperintensity, were found bilaterally in the hippocampi (arrow in Fig. 6A at the level 5.6 mm from bregma; the area of damage extends to levels 4.1 and 2.6 mm) and in other brain regions, including the amygdala and periamygdaloid cortex, endopiriform nucleus, ventral subiculum, EC and piriform cortex (located at level 8.6 mm), and the insular cortex (7.1 mm from bregma) in pilocarpine-treated rats 24 hours after a 180-minute SE (n = 3). Interestingly, the bright zones enlarged from the ventral (5.6 mm) to the dorsal (2.6 mm) hippocampal levels (20).

The evolution of bright zones depended on whether SE was interrupted at 120, 60, or 30 minutes from its onset (Fig. 6B). Bright areas of signal hyperintensity (arrows in T2W images) were detectable in the hippocampus 24 hours after a 120-minute SE (n = 7) and increased in size 1 day later. In contrast, after 60-minute SE (n = 6), the bright zones appeared only 48 hours after pilocarpine treatment, whereas animals that had experienced a 30-minute SE (n = 6) exhibited T2W hyperintensity in the hippocampus 72 hours after SE (Fig. 6C). Apparent diffusion coefficient maps (Figs. 6B, C) also revealed regions of hypointensity (arrows in Tr(D) images) in the core of T2W hyperintense areas in the hippocampus, suggesting cytotoxic edema (21). Both magnetic resonance imaging changes were prevented by protecting rats (n = 6) exposed to 30-minute SE by the administration of diazepam (20 mg kg^{-1} 24 $hours^{-1}$) for 3 days, starting 24 hours after SE (Fig. 6C).

Protective Effects of Diazepam Treatment

We next determined whether preventing CA3 lesions by post-SE administration of diazepam affected the length of the latent period or the seizure frequency. Of 14 rats subjected to 30-minute SE and then protected with diazepam, 12 became epileptic. Within the first 9 days after SE, 50% of these epileptic animals exhibited spontaneous seizures. Similarly, 50% of rats exposed to 120-minute SE (n = 18) developed spontaneous seizures within 10 days after pilocarpine injection, and all became epileptic in approximately 4 weeks. The curves of seizure appearance, analyzed by the logrank test, were similar in these 2 groups of pilocarpine-treated rats (Fig. 6D); however, rats exposed to 30-minute SE followed by diazepam exhibited a lower seizure frequency compared with the animals exposed to 120-minute SE; this difference was significant during the first ($p < 0.01$) and last ($p < 0.05$) 10-day periods of observation (Fig. 6E).

To investigate the efficacy of diazepam neuroprotection in preventing CA3 lesions further, we performed neuron-specific nuclear protein, mGluR2/3, GFAP, laminin, and MAP2 (a neuronal marker of ischemic lesions; [22]) immunostaining in the stratum lacunosum–moleculare of animals exposed to 30-minute SE followed by diazepam and then killed 7 days later. As shown in Figure 7, diazepam treatment prevented the appearance of the CA3 lesion in 9 of 16 pilocarpine-injected animals. The criterion used to differentiate damaged from protected rats was the presence of an area of reduced GFAP extending bilaterally for more than 1 brain level (>300 μm). In the animals in which neuroprotection was not

attained, the lesions showed increased laminin immunoreactivity and disappearance of GFAP-positive astrocytes in the same area; these findings were similar to those observed in animals exposed to a longer SE (Fig. 2). Although the neuronal cell bodies, identified by the neuron-specific nuclear protein immunostaining, were preserved both in CA3 and DG (in which we did not detect any damage in the upper blade), we nevertheless noticed, enclosed within the area of reduced GFAP, regions devoid of MAP2 and mGluR2/3 immunoreactivities, suggesting damage to distal dendrites of pyramidal cells and to PP terminal fibers of the EC-projecting neurons, respectively (Fig. 7). Although we found no sign of damage in neuroprotected animals, we detected reactive astrocytes surrounding dilated blood vessels in the stratum lacunosum–moleculare of CA3 (see the GFAP immunostaining in the central column of Fig. 7), suggesting enhanced vulnerability of this region.

Detection of the CA3 Lesion in Young Rats

We next examined whether the probability of developing CA3 lesions was further reduced in young (3-week-old) compared with adult (8-week-old) animals both exposed to 60-minute SE (Fig. 8). We limited SE to 60 minutes because this time interval resulted in optimal survival for young animals, whereas it induced CA3 lesions in all adult rats (Fig. 6). Our aim was to obtain 2 different populations of rats that could be discriminated on the basis of the integrity of the direct PP pathway to examine the involvement of CA3 pyramids in epileptic activity. All adult pilocarpine-treated rats (n = 18) exhibited lesions in the CA3 hippocampal subfield that were characterized by a marked disappearance of GFAP (not shown) and MAP2 immunostaining (Fig. 8A). Immunoreactivity for mGluR2/3 in the same area was also reduced, corresponding to loss of Black-Gold–labeled myelinated fibers (arrowheads in Figs. 8A and B). In contrast, in young animals, the CA3 stratum lacunosum–moleculare was less frequently damaged; only 6 of 26 rats showed bilateral loss of GFAP immunoreactivity in more than 1 brain level (Fig. 8C). The GFAP-unstained areas also exhibited loss of immunoreactivity for mGluR2/3 receptors in 6 of 26 rats, suggesting that the PP terminal field was damaged in these animals. In contrast, using the neuronal marker MAP2, which clearly stained neuronal dendrites in control rats (Fig. 7), we did not detect any loss in immunoreactivity in the young group (Fig. 8A); this suggests that pyramidal cells were not damaged in these animals.

The extent of damage, quantified in the various groups of pilocarpine-treated rats as the volume of GFAP, mGluR2/3, and MAP2 disappearance in CA3, is illustrated in Figure 8D. Overall, the volume of GFAP loss roughly corresponded to the sum of MAP2 and mGluR2/3 lesion volumes in adult rats or to mGluR2/3 in the young group. This suggests that the lesion developed from the outmost region of stratum lacunosum–moleculare toward the pyramidal cell layer. In adult rats that had experienced 60-minute SE, the average lesion size (evaluated with GFAP immunostaining) was 3-fold larger than that in the neuroprotected group and 7-fold larger than that in young damaged rats. For all of the markers, the areas of loss of immunoreactivity in CA3 were significantly lower in neuroprotected adults and young rats compared with animals exposed to 60-minute SE ($p < 0.01$; Fig. 8D).

We next examined the time to onset and frequency of spontaneous seizures in both age groups. Adult rats developed Stage 5 spontaneous seizures starting from the first week after SE and invariably (n = 11) became spontaneously epileptic within a month from the pilocarpine injection (Fig. 9A). In contrast, only 2 of 10 pilocarpine-treated young rats exhibited Stage 5 spontaneous seizures starting 3 weeks after SE. The remaining young animals had only Stage 1 to 2 spontaneous seizures. The frequency of Stage 5 seizure in adult rats was similar to that observed in young rats measured 3 weeks after SE.

Recruitment of CA3 Pyramids in Seizure Activity by SE Reinduction

We next examined whether a lesion of the PP terminal field in CA3 was associated with a decreased probability of CA3 activation during seizures. Because of the very low occurrence of Stage 5 spontaneous seizures in young rats, we provoked seizures by reinjecting subthreshold doses of pilocarpine as suggested by Glien et al (12). All animals developed seizures after pilocarpine; however, 8 of 10 young rats exhibited SE after a single pilocarpine (200 mg kg^{-1}) injection, whereas only 3 of 15 adults developed SE with the same dose (Fig. 9A). In addition, after repeated pilocarpine injections, some of the remaining adult rats displayed only discontinuous seizure activity (n = 8), whereas others (n = 4) finally developed SE. Latency to SE was also shorter in the young group of epileptic rats but not statistically different from the adult group. Of 10 control nonepileptic 8-week-old rats treated with this procedure, 6 developed SE after repeated injections. This group was statistically different from young epileptic rats with respect to threshold ($p < 0.01$) and latency ($p < 0.05$).

In this series of experiments, both young and adult animals were killed 24 hours after pilocarpine to examine the possible induction of FosB/ΔFosB immunoreactivity in the CA3 subfield. As previously reported (7), FosB/ΔFosB immunoreactivity was induced in all regions of the hippocampal formation in control animals. Young epileptic rats were similar, although areas devoid of positive cells were identified in relation to previous cell loss (Fig. 9B; medial entorhinal cortex Layer III). In particular, the CA3 pyramidal layer of young rats (~80%) exposed to the second SE was FosB/ΔFosB-immunopositive, whereas only sparse cells were present in the adult group even in animals in which SE was reinstated (Fig. 9B). This difference in CA3 FosB/ΔFosB expression found in young and adult rats was not explained by differences in the integrity of the CA3 pyramidal layer, as shown by neuron-specific nuclear protein antibodies (Fig. 9B). FosB/ΔFosB immunostaining was also detected in the other brain regions of the hippocampal formation in both groups. On the other hand, a clear loss of the PP nerve terminals was evident in all adult rats, whereas it was found in only 2 animals (20%) in the young group (Fig. 9C). In these animals, the same in which we observed Stage 5 spontaneous recurrent seizures, we did not detect FosB-/ΔFosB-positive cells in the CA3 pyramidal layer.

DISCUSSION

We describe here a novel type of hippocampal lesion that is consistently observed in adult pilocarpine-treated rats exposed to at least 30-minute SE. This lesion causes disarrangement of the PP temporoammonic projection in CA3, contributing to abnormal function in this

region. In addition, with a 180-minute SE, the lesion enlarged, involving also the PP temporodentate fibers and granule cells found in the upper blade tip of dentate gyrus. This lesion was initially suggested by the presence of microhemorrhages surrounding dilated blood vessels, consistent with the development of vessel wall damage during SE. The presence of microhemorrhages was further supported by the appearance of an infiltrate of microglial cells positive for heme oxygenase 1, an enzyme typically induced by the presence of hemoglobin in the tissue (15). Microhemorrhages were also found in extrahippocampal areas such as the hypothalamus and thalamus of rats exposed to 180-minute SE, indicating that they were not an exclusive feature of damage to the hippocampus. Nevertheless, 30-minute SE evoked microhemorrhages in the hippocampus of some animals but not in other brain regions. Cerebral hemorrhages are not unique to the pilocarpine model because they have also been described after kainic acid–induced SE both in the hippocampus and thalamus (23).

In addition to microhemorrhages, in the CA3 stratum lacunosum–moleculare, we identified other modifications typically found in brain areas of pannecrosis (17, 18, 24). Among these changes, the finding of increased laminin immunostaining in the basement membrane of some blood vessels is intriguing. This result may indicate angiogenesis that was presumably triggered by blood-brain barrier damage, as recently shown in the pilocarpine model and in tissue from TLE patients (25). This interpretation is consistent with the increased laminin immunostaining in regions in which we did not find pannecrosis. Alternatively, increased laminin immunoreactivity can be interpreted as the consequence of degradation of the basement membrane caused by release of proteases in damaged blood vessels (16). This phenomenon is also observed in brain regions exposed to ischemia (26). Interestingly, ischemia has recently been identified in the neocortex of pilocarpine-treated rats (27). Indeed, the lesion described in the hippocampus was characterized by the complete loss of GFAP and MAP2 immunoreactivities, as found in areas of ischemic/hemorrhagic brain damage (17, 22, 24, 28).

We hypothesize that the CA3 lesion may alter the degree of pyramidal cell activation, thus altering the hippocampal network that drives seizure activity (7). Accordingly, the pannecrotic lesion we found in pilocarpine-treated animals was associated with decreased responsiveness of CA3 pyramids during SE reinduction; in fact, they did not show FosB/ΔFosB immunoreactivity. Similarly, Peng and Houser (6) have found a very low expression of c-Fos in CA3 at the onset of spontaneously recurrent seizures in pilocarpine-treated mice. In contrast, active pyramidal neurons were clearly immunostained for FosB/ΔFosB in the other hippocampal regions such as CA1 and the subiculum. A switch in the hippocampal circuitry (including the subiculum) from the trisynaptic to a monosynaptic dialog with the EC has been suggested in previous studies (29, 30). According to this hypothesis, the CA3 region can play a critical role by decreasing the probability of relaying epileptic discharges to CA1 (30).

Several lines of evidence also support the hypothesis that the excitatory transfer via the dentate gyrus is decreased in epileptic rats (8, 31). When we compared the effects of dentate gyrus stimulation in pilocarpine-treated rats versus controls, we found significantly reduced responses in the epileptic CA3 (7). Ang et al (30) have also reported that even a PP burst

stimulation protocol is unable to activate the CA3 subfield over control values in pilocarpine-treated epileptic rats. Although this result has been interpreted as the consequence of a well-preserved gate-keeping function in the epileptic dentate gyrus, it can also be related to the degree of maintenance of PP direct projections to CA3 (32). In fact, it has been reported in the normal brain that activation of CA3 pyramidal neurons after mossy fiber stimulation depends to a great extent on feed forward excitatory inputs arising from direct PP fibers localized in the stratum lacunosum–moleculare (33). Thus, we suggest that the severe PP lesion identified in pilocarpine-treated animals may impede CA3 activation in response to inputs arriving through the trisynaptic pathway. This effect can be accentuated by the apical dendrite lesion identified in CA3 pyramidal cells with MAP2 immunostaining.

In TLE patients and pilocarpine-treated rats, the medial EC is selectively damaged in Layer III, which is composed by neurons projecting to CA1 and the subiculum (34, 35). Neurons projecting to the dentate gyrus and CA3 are instead located in the spared Layer II (7, 34, 35). Accordingly, both young and adult rats showed intense FosB/ΔFosB immunoreactivity in the EC Layer II after SE reinduction. However, the CA3 subfield of adult rats was unstained, whereas the dentate gyrus displayed FosB/ΔFosB immunopositivity. These data suggest that EC Layer II neurons are active during spontaneous seizures, but the damage we identified in the stratum lacunosum-moleculare of this region precludes activation of CA3 pyramidal cells. This view is further supported by results showing FosB/ΔFosB immunoreactivity in the CA3 of young rats, a group that is more resistant to PP damage. Similarly to CA3, the dentate gyrus is also affected by the large lesion in the adult rats exposed to 180-minute SE. This involves both granule cells and PP fibers in the upper blade tip. In fact, Scharfman et al (36) found the upper blade to be less responsive to PP stimulation when compared with the lower blade.

The young animal group showed a decreased threshold to pilocarpine-induced SE compared with adult epileptic or control rats. Similar alterations in seizure threshold have been reported for rats exposed to kindling at P18 (37) or treated with lithium-pilocarpine at P10 (38) and later examined when they are adults. The decreased threshold to kainic acid-induced seizures documented in lithium-pilocarpine–treated rat pups is paralleled by downregulation of the ionotropic glutamate receptor subunits GluR1 and GluR2, as well as by overexpression of the excitatory amino acid carrier 1 (38). Nonetheless, despite this increased sensitivity to convulsants, the young rats in our study had less severe seizures when they became epileptic, as has also been found in other studies (39). According to Sankar et al (39), differences in time to the first seizure are not explained by the extent of the lesion. We also did not notice differences in young and adult rats exposed to 60-minute SE apart from the CA3 stratum lacunosum-moleculare.

We found the response to SE reinduction to be impaired in the group of adult rats, which showed more pronounced damage to EC-CA3 connections. Notably, the findings in the adult group are similar to those in rats with ablated lateral EC, which are less responsive to drug-induced seizures (40). This result was interpreted as a direct consequence of lateral EC damage because the EC is a critical region for ictogenesis both in humans and animal models of TLE (1). When EC-damaged rats developed seizures in response to 4-aminopyridine, however, they displayed a significantly longer tonic component than sham

animals, indicating that loss of EC inputs to the hippocampus results in more severe seizures (40). Conversely, Zhang et al (41) showed that rats treated with multiple subthreshold kainic acid and pilocarpine injections, which did not develop neuronal damage during SE, presented less frequent seizures than rats in which SE was associated with neuronal loss. These data are in line with our observations showing a higher seizure frequency and a more damaged PP terminal field in rats undergoing 120-minute SE compared with those exposed to 30-minute SE.

In conclusion, we have identified in adult pilocarpine-treated epileptic rats a novel neuronal network damage developing just after a 30-minute SE. The nature of this lesion is probably ischemic, as suggested by loss of staining for neuronal soma and fiber markers, as well as by the disappearance of astrocytes and damage to vessel walls. Apparently, the presence of this lesion is consistently associated with more severe seizures. In particular, the adult animals damaged both in the CA3 stratum lacunosum–moleculare and in the dentate gyrus upper blade had more frequent seizures than the animals with damage only in CA3. In addition, the young animals were resistant to both lesions and presented a delayed development of generalized seizures. These data suggest the existence of a gradient in seizure severity that is explained by the extent of the PP lesion. Furthermore, hippocampal sclerosis is associated with intractable seizures in TLE patients (2). It remains to be established whether the changes we described in the pilocarpine model occur in the hippocampus of TLE patients and whether these changes aggravate seizures or limit the efficacy of drug treatment in these individuals.

Acknowledgments

This study was supported by Grant No. R-06-50 from the Pierfranco and Maria Luisa Mariani Foundation, Grant No. 1232 PRIER 2007/09 from the Emilia-Romagna Region, Grant No. MT-8109 from the Canadian Institutes of Health Research, and the Savoy Foundation. Enrica Baldelli was recipient of a Mariani Foundation–University of Modena and Reggio Emilia Fellowship (Borsa di Studio per la Ricerca e Formazione Avanzata 2006/07).

References

1. Avoli M, D'Antuono M, Louvel J, et al. Network and pharmacological mechanisms leading to epileptiform synchronization in the limbic system. Prog Neurobiol. 2002; 68:167–207. [PubMed: 12450487]
2. Pitkanen A, Sutula TP. Is epilepsy a progressive disorder? Prospects for new therapeutic approaches in temporal-lobe epilepsy. Lancet Neurol. 2002; 1:173–81. [PubMed: 12849486]
3. Morimoto K, Fahnestock M, Racine RJ. Kindling and status epilepticus models of epilepsy: Rewiring the brain. Prog Neurobiol. 2004; 73:1–60. [PubMed: 15193778]
4. Willoughby JO, Mackenzie L, Medvedev A, et al. Fos induction following systemic kainic acid: Early expression in hippocampus and later widespread expression correlated with seizure. Neuroscience. 1977; 77:379–92.
5. Hsieh PF, Watanabe Y. Time course of c-FOS expression in status epilepticus induced by amygdaloid stimulation. Neuroreport. 2000; 11:571–74. [PubMed: 10718316]
6. Peng Z, Houser CR. Temporal patterns of fos expression in the dentate gyrus after spontaneous seizures in a mouse model of temporal lobe epilepsy. J Neurosci. 2005; 25:7210–20. [PubMed: 16079403]
7. Biagini G, D'Arcangelo G, Baldelli E, et al. Impaired activation of CA3 pyramidal neurons in the epileptic hippocampus. Neuromol Med. 2005; 7:325–42.

8. Gutiérrez R, Heinemann U. Kindling induces transient fast inhibition in the dentate gyrus-CA3 projection. Eur J Neurosci. 2001; 13:1371–79. [PubMed: 11298797]
9. Biagini G, Baldelli E, Longo D, et al. Endogenous neurosteroids modulate epileptogenesis in a model of temporal lobe epilepsy. Exp Neurol. 2006; 201:519–24. [PubMed: 16780839]
10. Liu Z, Stafstrom CE, Sarkisian MR, et al. Seizure-induced glutamate release in mature and immature animals: An in vivo microdialysis study. Neuroreport. 1997; 8:2019–23. [PubMed: 9223095]
11. Racine RJ. Modification of seizure activity by electrical stimulation. II. Motor seizure. Electroencephalogr Clin Neurophysiol. 1972; 32:281–394. [PubMed: 4110397]
12. Glien M, Brandt C, Potschka H, et al. Repeated low-dose treatment of rats with pilocarpine: Low mortality but high proportion of rats developing epilepsy. Epilepsy Res. 2001; 46:111–19. [PubMed: 11463512]
13. Schmued L, Slikker W Jr. Black-gold: A simple, high-resolution histochemical label for normal and pathological myelin in brain tissue sections. Brain Res. 1999; 837:289–97. [PubMed: 10434014]
14. Biagini G, Sala D, Zini I. Diethyldithiocarbamate, a superoxide dismutase inhibitor, counteracts the maturation of ischemic-like lesions caused by endothelin-1 intrastriatal injection. Neurosci Lett. 1995; 190:212–16. [PubMed: 7637895]
15. Wu J, Hua Y, Keep RF, et al. Iron and iron-handling proteins in the brain after intracerebral hemorrhage. Stroke. 2003; 34:2964–69. [PubMed: 14615611]
16. Chen Z-L, Strickland S. Neuronal death in the hippocampus is promoted by plasmin-catalyzed degradation of laminin. Cell. 1997; 91:917–25. [PubMed: 9428515]
17. Wegener S, Weber R, Ramos-Cabrer P, et al. Temporal profile of T2-weighted MRI distinguishes between pannecrosis and selective neuronal death after transient focal cerebral ischemia in the rat. J Cereb Blood Flow Metab. 2006; 26:38–47. [PubMed: 15988477]
18. Auer RN, Siesjo BK. Biological differences between ischemia, hypoglycemia, and epilepsy. Ann Neurol. 1988; 24:699–707. [PubMed: 3061362]
19. Pacheco Otalora LF, Couoh J, Shigamoto R, et al. Abnormal mGluR2/3 expression in the perforant path termination zones and mossy fibers of chronically epileptic rats. Brain Res. 2006; 1098:170–85. [PubMed: 16793029]
20. Paxinos, G., Watson, C. The Rat Brain in Stereotaxic Coordinates. 6. Amsterdam, The Netherlands: Elsevier; 2007.
21. Guerrini U, Sironi L, Tremoli E, et al. New insights into brain damage in stroke-prone rats: A nuclear magnetic imaging study. Stroke. 2002; 33:825–30. [PubMed: 11872910]
22. Kuhn J, Meissner C, Oehmichen M. Microtubule-associated protein 2 (MAP2)—A promising approach to diagnosis of forensic types of hypoxia-ischemia. Acta Neuropathol. 2005; 110:579–86. [PubMed: 16328528]
23. Sloviter RS. The neurobiology of temporal lobe epilepsy: Too much information, not enough knowledge. C R Biol. 2005; 328:143–53. [PubMed: 15771000]
24. Zoli M, Biagini G, Ferrari R, et al. Neuronglia cross talk in rat striatum after transient forebrain ischemia. Adv Exp Med Biol. 1997; 429:55–68. [PubMed: 9413565]
25. Rigau V, Morin M, Rousset MC, et al. Angiogenesis is associated with blood-brain barrier permeability in temporal lobe epilepsy. Brain. 2007; 130:1942–56. [PubMed: 17533168]
26. Yepes M, Sandkvist M, Wong MK, et al. Neuroserpin reduces cerebral infarct volume and protects neurons from ischemia-induced apoptosis. Blood. 2000; 96:569–76. [PubMed: 10887120]
27. Fabene PF, Merigo F, Galiè M, et al. Pilocarpine-induced status epilepticus in rats involves ischemic and excitotoxic mechanisms. Plos One. 2007; 2:e1105. [PubMed: 17971868]
28. Biagini G, Zoli M, Torri C, et al. Protective effects of delapril, indapamide and their combination chronically administered to stroke-prone spontaneously hypertensive rats fed a high-sodium diet. Clin Sci. 1997; 93:401–11. [PubMed: 9486085]
29. D'Antuono M, Benini R, Biagini G, et al. Limbic network interactions leading to hyperexcitability in a model of temporal lobe epilepsy. J Neurophysiol. 2002; 87:634–49. [PubMed: 11784779]

30. Ang CW, Carlson GC, Coulter DA. Massive and specific dysregulation of direct cortical input to the hippocampus in temporal lobe epilepsy. J Neurosci. 2006; 26:11850–56. [PubMed: 17108158]

31. Goussakov IV, Fink K, Elger CE, et al. Metaplasticity of mossy fiber synaptic transmission involves altered release probability. J Neurosci. 2000; 20:3434–41. [PubMed: 10777806]

32. Wu K, Leung L-WS. Monosynaptic activation of CA3 by the medial perforant path. Brain Res. 1998; 797:35–41. [PubMed: 9630498]

33. Urban NN, Henze DA, Barrionuevo G. Revisiting the role of the hippocampal mossy fiber synapse. Hippocampus. 2001; 11:408–17. [PubMed: 11530845]

34. Witter MP, Groenewegen HJ, Lopes da Silva FH, et al. Functional organization of the extrinsic and intrinsic circuitry of the parahippocampal region. Prog Neurobiol. 1989; 33:161–253. [PubMed: 2682783]

35. Du F, Whetsell WO, Abou-Khalil B, et al. Preferential neuronal loss in layer III of the entorhinal cortex in patients with temporal lobe epilepsy. Epilepsy Res. 1993; 16:223–33. [PubMed: 8119273]

36. Scharfman HE, Sollas AL, Smith KL, et al. Structural and functional asymmetry in the normal and epileptic rat dentate gyrus. J Comp Neurol. 2002; 454:424–39. [PubMed: 12455007]

37. Moshé SL, Albala BJ. Kindling in developing rats: Persistence of seizures into adulthood. Brain Res. 1982; 256:67–71. [PubMed: 7093730]

38. Zhang G, Raol YS, Hsu FC, et al. Long-term alterations in glutamate receptor and transporter expression following early-life seizures are associated with increased seizure susceptibility. J Neurochem. 2004; 88:91–101. [PubMed: 14675153]

39. Sankar R, Shin DH, Liu H, et al. Patterns of status epilepticus-induced neuronal injury during development and long-term consequences. J Neurosci. 1998; 18:8382–93. [PubMed: 9763481]

40. Kopniczky Z, Dobo E, Borbely S, et al. Lateral entorhinal cortex lesions rearrange afferents, glutamate receptors, increase seizure latency and suppress seizure-induced c-fos expression in the hippocampus of adult rat. J Neurochem. 2005; 95:111–24. [PubMed: 16181416]

41. Zhang X, Cui SS, Wallace AE, et al. Relations between brain pathology and temporal lobe epilepsy. J Neurosci. 2002; 22:6052–61. [PubMed: 12122066]

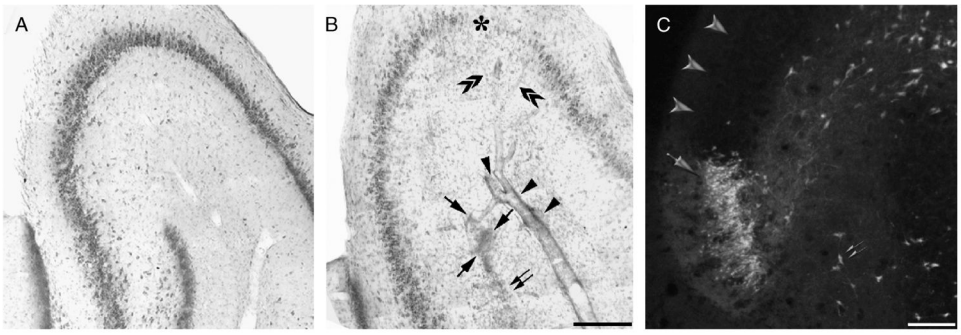

FIGURE 1.

Photomicrographs illustrating the presence of a focal hemorrhagic lesion centered in the CA3 stratum lacunosum–moleculare 1 week after exposure to 180 minutes of status epilepticus (SE). **(A, B)** Toluidine blue staining of the CA3 region in a nonepileptic control animal **(A)** and in a pilocarpine-treated rat **(B)**. **(B)** Note the presence of perivascular extravasated erythrocytes (arrowheads) and focal hemorrhages (arrows) close to an area of granule cell disappearance in the dentate gyrus (double arrow); an area of marked cell loss in CA3 (asterisk) is reached by dilated branches (double arrowheads) of the vessel surrounded by the microhemorrhages. **(C)** A cluster of necrotic cells visualized by the Fluoro-Jade method in the upper blade of the dentate gyrus 3 days after SE (**C**; arrow); only a few positively stained cells are identified outside of the lesion (arrowheads) or in the dentate hilus (double arrowhead). Scale bars = **(A, B)** 300 μm; **(C)** 100 μm.

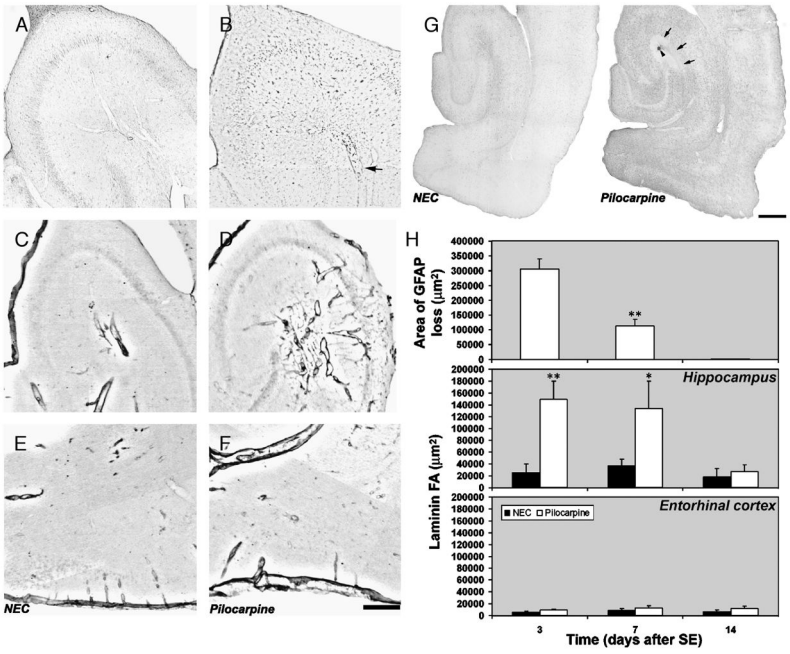

FIGURE 2.

Changes in immunoreactivity of markers for glial cells and blood vessel wall. **(A, B)** Distribution of immunoreactivity for heme oxygenase-1 in a control rat **(A)** and in a pilocarpine-treated rat **(B)**; the arrow points to a dilated blood vessel in which many heme oxygenase-1-positive cells can be identified. Immunoreactivity for laminin in basal condition **(C, E)** and in a pilocarpine-treated rat **(D, F)** in CA3 **(C, D)** and in the entorhinal cortex **(E, F)**. **(G)** Distribution of glial fibrillary acidic protein (GFAP)-positive astrocytes in a control rat. In the pilocarpine-treated rat, note the clear-cut area devoid of immunoreactivity in the CA3 stratum lacunosum-moleculare (arrows) surrounding a focal microhemorrhage (arrowhead). **(H)** The top panel shows the quantification of the area of GFAP loss after status epilepticus (SE). *, $p < 0.01$ versus 3 days after SE group using analysis of variance, followed by the least-significant-difference test for multiple comparisons. Quantification of laminin immunoreactivity is shown in middle and bottom panels. *, $p < 0.05$; **, $p < 0.01$ versus controls. Analysis of variance, followed by the least-significant-difference test for multiple comparisons. Scale bars = **(A–F)** 300 µm; **(G)** 500 µm. NEC, nonepileptic control.

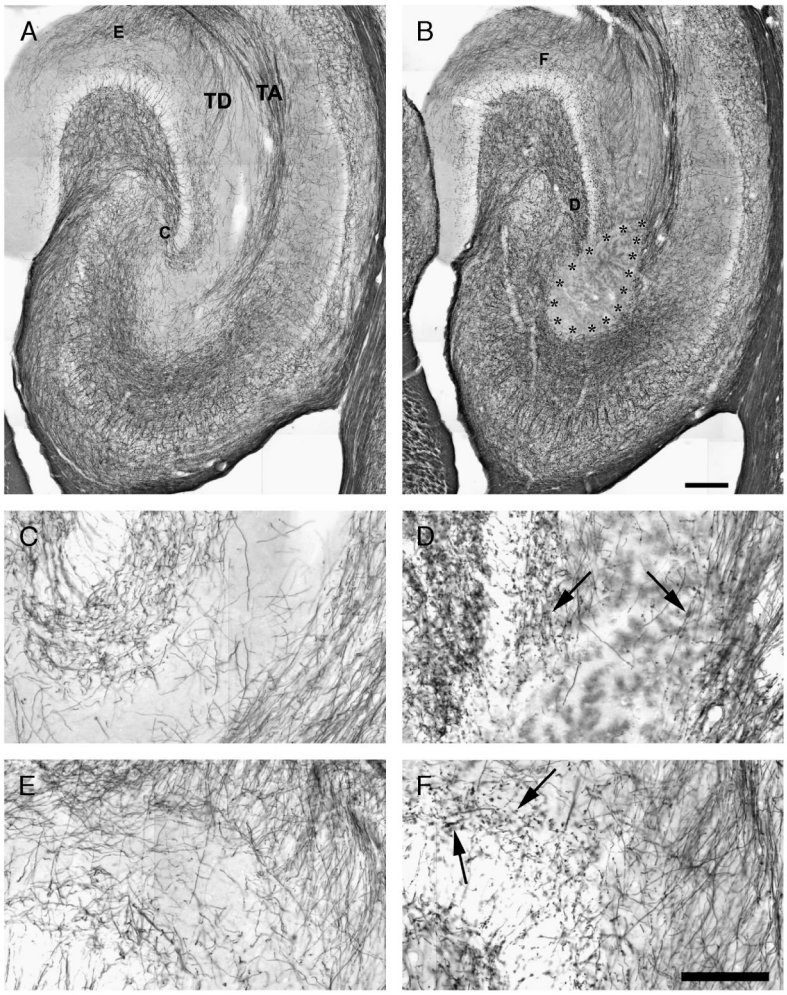

FIGURE 3.

Staining of nerve fibers with the Black-Gold method in a nonepileptic control animal **(A)** and in a pilocarpine-treated rat with a large lesion (delimited by asterisks) in the CA3 stratum lacunosum-moleculare **(B)**. **(A)** The perforant path (PP) projection is clearly detectable and consists either of fibers crossing the hippocampal fissure to reach the dentate gyrus molecular layer (TD) or fibers crossing the hippocampus and terminating in the CA3 stratum lacunosum-moleculare (TA). **(C–F)** Show the regions magnified in the following panels. **(C, D)** Magnification of PP nerve fibers in CA3, in control, and in pilocarpine-treated rats. **(D)** Note the fiber loss and the presence of punctuate stained beads and varicosities (arrows). **(E, F)** Details of PP nerve fibers reaching the dentate gyrus are shown in control **(E)** and pilocarpine-treated rats **(F)**. Note the presence of intensely stained nerve fiber beads and varicosities (arrows) **(F)**. Scale bars = **(A, B)** 250 μm; **(C–F)** 100 μm. TA, temporoammonic projection; TD, temporodentate projection.

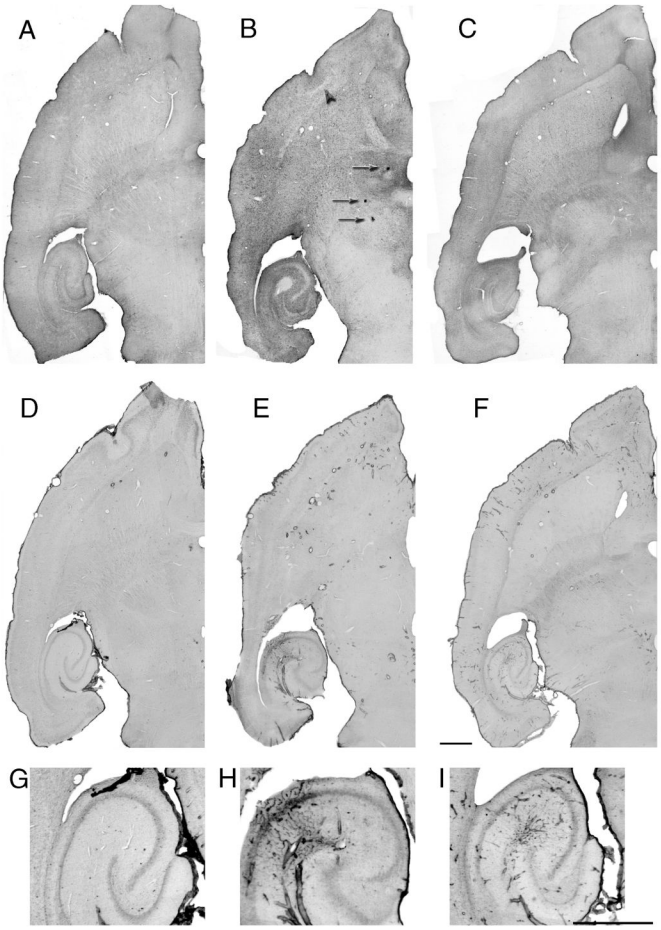

FIGURE 4.

Lesions in extrahippocampal regions. **(A)** The immunostaining with a polyclonal antibody against glial fibrillary acidic protein (GFAP) is shown in a control animal. **(B)** Glial fibrillary acidic protein immunostaining reveals a focal area devoid of immunoreactivity in the hippocampus of a rat exposed to 180-minute status epilepticus (SE). There is also an irregular zone almost devoid of GFAP-positive cells at the boundary between the piriform and insular cortices (arrowhead). Microhemorrhages are visible in the hypothalamus and thalamus (arrows). Hemorrhagic lesions were not present when SE was limited to 30 minutes **(C)**. In sections close to those used for GFAP immunostaining, laminin immunoreactivity was increased in the basement membrane of blood vessels of rats exposed to 180- **(E)** or to 30-minute **(F)** SE compared with a control **(D)**. The increase in laminin immunostaining was clearly focal (**H** and **I** are higher magnifications of the hippocampi shown in **E** and **F**, respectively). The hippocampus of a control rat is shown **(G)**. Scale bars = 1 mm.

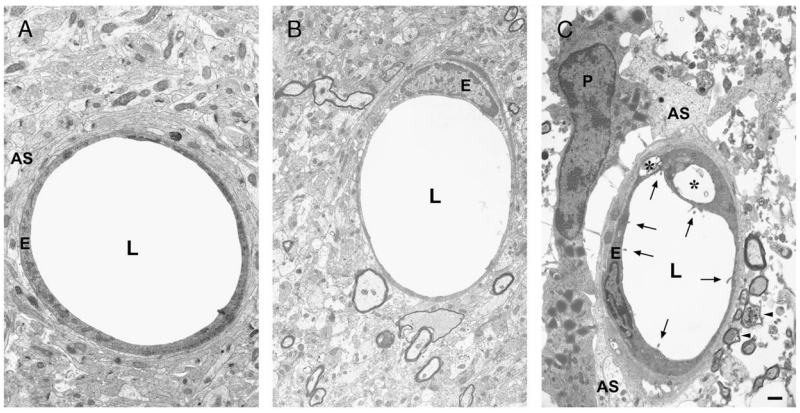

FIGURE 5.

Electron photomicrographs of vascular lesions in the CA3 of rats exposed to 30 minutes of status epilepticus (SE) and killed 1 to 3 days later. **(A)** A blood vessel with preserved morphology from a control nonepileptic rat; astrocytic end-foot processes (ASs) are close to endothelial cells (Es) delimiting the vessel wall. **(B)** A pilocarpine-treated rat studied 1 day after SE. **(C)** A pilocarpine-treated rat 3 days after SE. The capillary shows reduction in the lumen (L). There are several microvilli on the surface of endothelial cells (arrows) and large vacuoles within their cytoplasm (asterisks). There is also an apparently migrating pericyte (P), marked edema of ASs, and axon degeneration (arrowheads). Scale bar = 1 μm (original magnification, ×4,000).

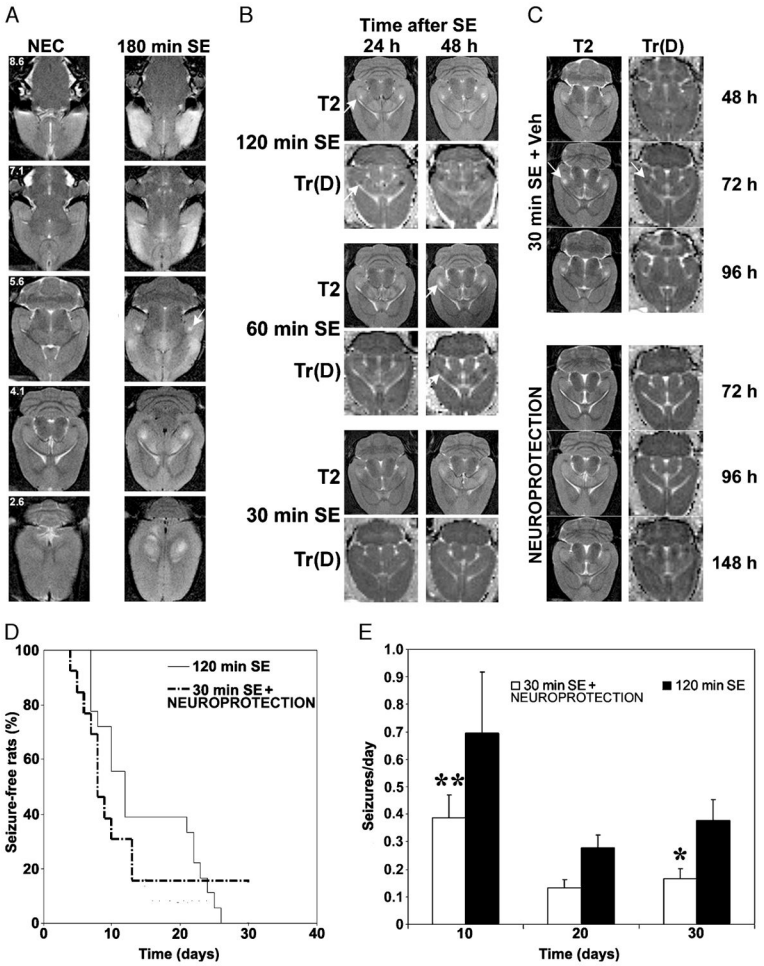

FIGURE 6.

Nuclear magnetic resonance imaging illustrating the distribution of brain lesions after status epilepticus (SE) in pilocarpine-treated rats and neuroprotection with diazepam. **(A)** Horizontal T2-weighted (T2W) images from bregma level 8.6 to 2.6 mm (20) are shown for an nonepileptic control (NEC) rat and a pilocarpine-treated rat exposed to 180-minute SE. Note the appearance of hyperintense signals in several brain regions, including the hippocampal CA3 subfield (5.6; arrow). **(B)** The hyperintense signals in T2W and the hypointense signals in Tr(D) images are progressively delayed by shortening the SE duration (arrows). **(C)** Hyperintense signals in T2W and hypointense signals in Tr(D) images are observed in rats exposed to 30-minute SE 72 hours after pilocarpine injection. Neuroprotection of these animals with repeated diazepam administration prevented the changes in signal intensities. **(D)** Rats exposed to 30-minute SE and neuroprotected developed spontaneous recurrent seizures with a time course similar to that seen in rats exposed to 120-minute SE. **(E)** The seizure frequency seemed to be significantly lower in rats exposed to 30-minute SE. *, $p < 0.05$, **, $p < 0.01$; analysis of variance followed by the least-significant-difference test for multiple comparisons.

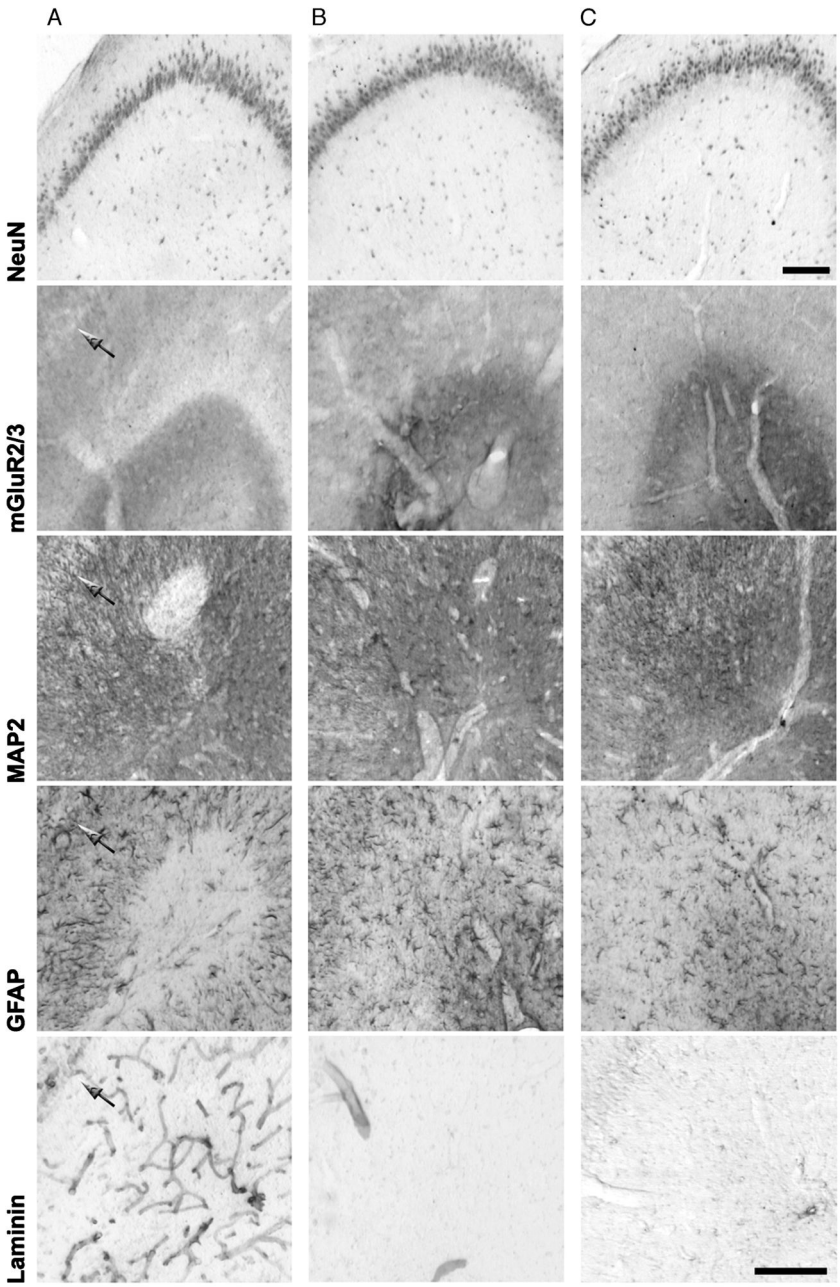

FIGURE 7.

Protective effects of repeated diazepam treatment in pilocarpine-treated rats exposed to 30-minute status epilepticus (SE). The lesion was investigated with antibodies against neuronal (neuron-specific nuclear protein [NeuN]; metabotropic glutamate receptor 2/3 [mGluR2/3]; microtubule-associated protein 2 [MAP2]), glial (glial fibrillary acidic protein [GFAP]) and blood vessel (laminin) antigens in serial sections of pilocarpine-treated and control rats. Frames shown (**A**; defective neuroprotection) illustrate a rat in which diazepam did not preclude the development of damage in the CA3 stratum lacunosum-moleculare. The arrows indicate the pyramidal cell layer in the respective frames. (**B**; effective neuroprotection) A

pilocarpine-treated rat that experienced 30-minute SE in which the protocol of diazepam administration prevented the appearance of unstained areas and increased laminin immunoreactivity. The control is shown **(C)**. Scale bars = 150 μm.

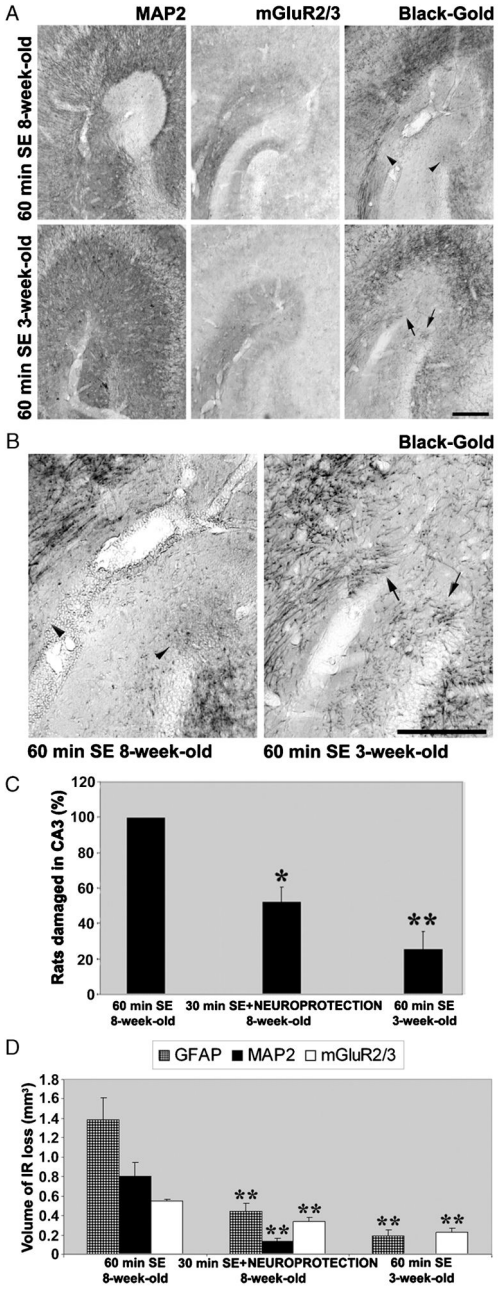

FIGURE 8.

Photomicrographs of the CA3 lesion occurring after exposure to 60-minute status epilepticus (SE) in serial sections of adult (8-week-old) and young (3-week-old) rats. **(A)** The CA3 lesion is identified in adult 8-week-old rats by microtubule-associated protein 2 (MAP2) and metabotropic glutamate receptor 2/3 (mGluR2/3) staining. The correlation of mGluR2/3 immunoreactivity to disappearance of perforant path axons was confirmed using Black-Gold staining (arrowheads). This staining is shown at higher magnification **(B)**. The fibers were detected in the young animals (arrows). **(C)** Bars indicate the percentages of animals with the CA3 focal lesion. *, $p < 0.05$, **, $p < 0.01$ versus 8-week-old 60-minute SE group. **(D)**

Quantification of the volume of glial fibrillary acidic protein (GFAP), MAP2, and mGluR2/3 disappearance. **, $p < 0.01$ versus 8-week-old 60-minute SE group. Analysis of variance, followed by the least-significant-difference test for multiple comparisons were used **(C, D)**. Scale bars = 200 μm.

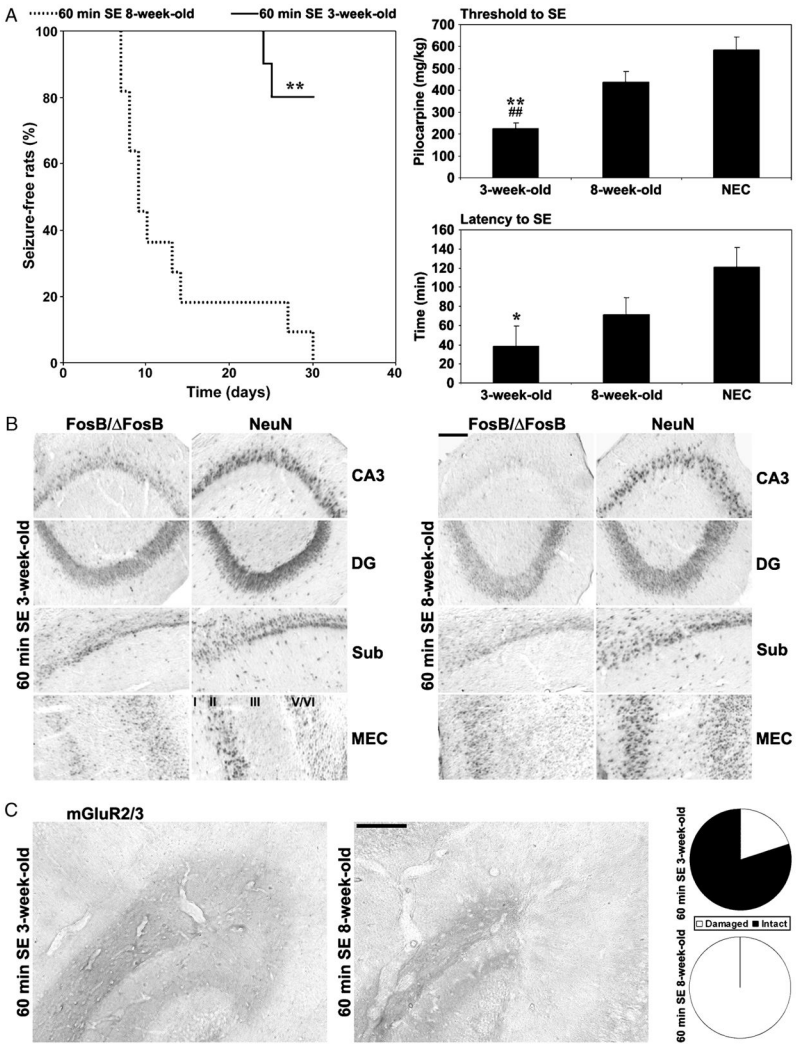

FIGURE 9.

Differences in epileptogenesis, status epilepticus (SE) reinduction, CA3 activation, and perforant path (PP) lesion in rats receiving the initial pilocarpine treatment when either 3 or 8 weeks old. **(A)** Kaplan-Meier analysis of period when spontaneous Racine Stage 5 seizures appeared (shown on the left; **, $p < 0.01$; logrank test). In the right panels, the effects of SE reinduction obtained by injecting subthreshold pilocarpine doses in the epileptic rats or in nonepileptic control (NEC) animals. In the top panel, SE reinduction reveals a significantly decreased threshold in the young (3-week-old) group of rats. The bottom panel shows a significantly lower latency. (*, $p < 0.05$, **, $p < 0.01$ versus NEC; $^{\#\#}$, $p < 0.01$ versus adult epileptic rats; analysis of variance, followed by the least-significant-difference test for multiple comparisons). **(B)** FosB/ΔFosB and neuron-specific nuclear protein (NeuN) immunostaining in serial sections of the hippocampal formation in young and adult epileptic rats 1 day after SE reinduction. FosB/ΔFosB immunoreactivity was found in the CA3 of 8 of 10 young rats. Differences in other areas or in NeuN staining are not evident. **(C)** Metabotropic glutamate receptor 2/3 (mGluR2/3)-immunostained perforant path nerve terminals in a young (left) and an adult (center) rat corresponding to the

respective FosB/ΔFosB immunostaining **(B)**. On the right, the percentage of animals with mGluR2/3 loss in stratum lacunosum-moleculare is indicated for each group. Scale bars = 150 μm. DG, dentate gyrus; MEC, medial entorhinal cortex; Sub, subiculum.

TABLE

Primary Antibodies Used to Identify Neuronal and Glial Cell Types and Blood Vessels

Antibodies	Source	Isotype	Clone	Code	Dilution	Supplier	Localization
FosB/ΔFosB	Rabbit polyclonal	IgG	H-75	sc-7203	1:250	Santa Cruz Biotechnology, Santa Cruz, CA	Neurons
GFAP	Rabbit polyclonal	IgG	—	Z 0334	1:500	DAKO, Glostrup, Denmark	Astrocytes
HO-1	Rabbit polyclonal	IgG	—	SPA-895	1:500	Stressgen, Victoria, British Columbia, Canada	Activated microglia
Laminin	Mouse monoclonal	IgG1	LAM-89	L8271	1:2000	Sigma-Aldrich, Milan, Italy	Basement membrane of blood vessels
MAP2	Mouse monoclonal	IgG1	HM-2	M4403	1:500	Sigma-Aldrich	Neurons
mGluR2/3	Rabbit polyclonal	IgG	—	AB1553	1:100	Chemicon, Temecula, CA	Neurons
NeuN	Mouse monoclonal	IgG1	A60	MAB377	1:100	Chemicon	Neurons

GFAP, glial fibrillary acidic protein; HO-1, heme oxygenase 1; Ig, immunoglobulin; MAP2, microtubule-associated protein 2; mGluR2/3, metabotropic glutamate receptor 2/3; NeuN, neuron-specific nuclear protein.